

Hybrid films of Co – C₆₀ preparation and changes induced by external stimuli.

Giovanni Ceccio^{1,*} , Jiri Vacik¹ , Yuto Kondo², Kazumasa Takahashi² , Romana Miksova¹ , Eva Stepanovska^{1,3} , Josef Novak^{1,3} , Petr Malinsky^{1,3} , Barbara Fazio⁴ , Catia Cannilla⁵ , Alena Michalcova⁶ , and Sebastiano Vasi^{7,8,*} 

¹ Department of Neutron and Ion Methods, Nuclear Physics Institute of Czech Academy of Science, Hlavní čp. 130 Husinec - Řež, 25068, Czech Republic

² Department of Electrical Engineering, Nagaoka University of Technology, 1603-1 Kamitomioka, Nagaoka, Niigata, 940-2188, Japan

³ Department of Physics, Faculty of Science, J. E. Purkyne University in Ústí nad Labem, Pasteurova 3632/15, 400 96 Ústí nad Labem, Czech Republic

⁴ IMM-CNR sede di Messina, Viale Ferdinando Stagno d'Alcontres, 31, 98166, Messina, Italy

⁵ CNR-ITAE, Istituto di Tecnologie Avanzate per l'Energia, Via S. Lucia Sopra Contesse 5, 98126, Messina, Italy

⁶ Department of Metals and Corrosion Engineering, University of Chemistry and Technology in Prague, Technicka 5, Prague 6, 166 28, Czech Republic

⁷ Department of Mathematics and Computer Sciences, University of Messina, Physical Sciences and Earth Sciences, Viale F. Stagno d'Alcontres 31, 98166, Messina, Italy

⁸ OPENFIS S.R.L. - SPIN OFF ACCADEMICO, Viale F. Stagno D'Alcontres 31, 98166, University of Messina, LABORATORIO A2AT3, Messina, Italy

* Author to whom any correspondence should be addressed.

E-mail: ceccio@ujf.cas.cz

Keywords: Cobalt, Fullerene, Thin film, Annealing, Ion irradiation

Abstract

In this work, we report on the study on organic-metal hybrid systems, in particular Co-C₆₀ fullerene thin films. This study mainly focused on the investigation of the morphological and structural evolution of the film surface after various external stimuli designed to provide energy to the system. For film growth, we adopted an innovative approach, combining ion-beam sputtering of a pure metal target with thermal evaporation of C₆₀ in a co-deposition setup. The films underwent a series of treatments to induce modifications. Laser and ion irradiations were performed using a pulsed laser, a continuous Ar beam, and a pulsed C beam. In addition, thermal annealing in vacuum was performed to examine the long-term effects of temperature. The composition of deposited film was investigated using Ion Beam Analysis, the morphology and the structure, and the effects of treatments on the films were studied using SEM and TEM microscopies and Raman spectroscopy. Changes in electrical resistance were also measured to explore potential applications of these films after treatment.

1 Introduction

Recent advances in nanoscience, particularly in nanoarchitectures, highlight metal-organic hybrid nanostructures as an increasingly relevant research topic, yielding intriguing results in electronics and proposing advanced applications, such as catalysis and electrochemistry, energy storage and conversion, gas sensing and spintronics [1–16]. The study of C₆₀ fullerene in such hybrid systems is often taken into consideration due to the unique properties of C₆₀ molecules, such as the exciting atomic structure, the intriguing coupling with metals, the tiny hyperfine interactions, the greater structural stability and the relative low cost. These features collectively increase the interest in such materials [17–22]. Among various C₆₀-based hybrid systems, self-assembled nanostructured materials are particularly notable for their tunability, offering precise control over the nanostructure during growth or post-production to tailor their electrical properties. The discovery of higher conductivity and superconductivity in alkali metal fullerides has also been a strong motivation for the implementation of transition metal-fullerene related research [20, 23–25]. Attempts to combine

transition metals (TM) and C₆₀ via co-deposition to access TM-fullerides have usually revealed pronounced metal clustering (due to the high cohesive energy of metals) with separation from C₆₀ phase, which hinders homogeneous mixing but also enables additional functional behaviour of such nanostructures [25, 26]. An example is given by structures based on the coexistence of Co and C₆₀, in both homogeneous compounds and heterogeneous films, which have a great impact in spintronics due to the catalytic and magnetic properties of Co [17, 27–31]. Furthermore, such hybrid systems have gained interest for potential applications in lithium-ion batteries [32], where structural stability, conductivity, and controlled phase evolution are critical for improving performance and longevity. Besides their interesting properties, however, integrated hybrid systems are considered thermodynamically and structurally unstable (mainly due to the high internal stress resulting from the mixing of mostly immiscible phases and the vulnerability of C₆₀ molecular cages due to their easy photo-oxidation, polymerization or fragmentation in an environment exhibiting strong catalytic properties) [33–35]. This makes their possible applications more challenging. The use of various disruptive agents (such as thermal annealing, ion irradiation, laser illumination, chemical reagents, etc.) can significantly influence thermodynamically unstable systems, inducing their structural changes at the nanoscopic and macroscopic scales as the system moves toward a state of minimum energy. This approach not only enables control over material properties for specific applications, but also serves as a model for studying the long-term evolution of these hybrid systems under extreme conditions, which is highly relevant for their potential integration into devices designed for harsh environments (e.g., space applications, high-radiation areas, and extreme temperature conditions). While numerous studies have investigated the growth, structure, and intrinsic properties of metal–C₆₀ hybrid systems, most reported works focus on as-deposited films or on single modification routes, often produced under different deposition conditions or with varying compositions [25, 27, 36]. As a result, a direct and systematic comparison of how different external stimuli influence the same Co–C₆₀ system remains limited [20]. The ability to intentionally modify the system provides the advantage of preventing unwanted changes due to system aging or adverse environmental conditions during the lifetime of a possible device based on such systems. Our previous systematic works [37–39] have focused on study the physical properties of systems realized using different ratios of constituents within thin films. In contrast to these previous studies, the present work does not aim to explore new compositions or mixing ratios, but rather to isolate the effects of different post-deposition energy inputs applied to films fabricated under strictly identical growth conditions. This post-treatment-centered approach allows us to disentangle how distinct excitation pathways drive structural reorganization and functional property changes in the same hybrid system. The prepared samples have been exposed to vacuum annealing, pulsed laser irradiation, and ion irradiation (continuous beam and pulsed beam). The analyses performed show that the hybrid systems evolved in different ways, exhibiting diversification in their nanostructures and macrostructures depending on the external perturbation applied.

2 Materials and Methods

We have produced a set of Co–C₆₀ mixture films by co-deposition of Co and C₆₀ on Si(110) substrates in high vacuum (base vacuum, 2E-6 mbar). The growth of the Co film was performed by the ion beam sputtering technique realized by using a Low Energy Ion Facility (LEIF) [32, 40], operating with a beam of Ar⁺ ions accelerated at 20 keV and focused on a Co target (2 inch x 0.125 inch, 99.99% purity, Kurt J. Lesker) mounted on a suitable target holder and inclined at 45 degrees with respect to the beam. The target faces the substrates mounted at a distance of 100 mm, under an angle of 30 degrees. Just below the substrate holder, at the distance of 100 mm, a lab made evaporator that acts as a source of C₆₀ (99.9% purity, Nanografi) is present, in order to perform simultaneous deposition of Co and C₆₀ (see sketch in Fig. 1). The evaporator, equipped with digital temperature control and a thermocouple inserted directly into the crucible, was maintained at a temperature of 450 °C for the entire duration of the deposition. During the beam calibration and heat up procedure of the crucible, a shutter is present to avoid unwanted depositions on the substrates. For TEM analytical purpose, samples were deposited on 300 mesh Cu TEM grids with holey carbon films (TedPella, Inc.).

All films were deposited together in order to guarantee the same experimental parameters and the same film on all substrates. Ion Beam Analysis experiments were performed at the Tandetron MC 4130 tandem accelerator located at NPI. RBS and ERDA were used for the analysis. To identify heavier elements, He⁺ ions with an energy of 2 MeV were used, while for the carbon detection H⁺ ions at 1.735 MeV were chosen, hitting the films with an incident angle of 7°. The backscattered ions were detected using an ORTEC ULTRA-series detector, which features a 50 mm² active area and a 300 μm thick depletion layer. The detector was positioned at a

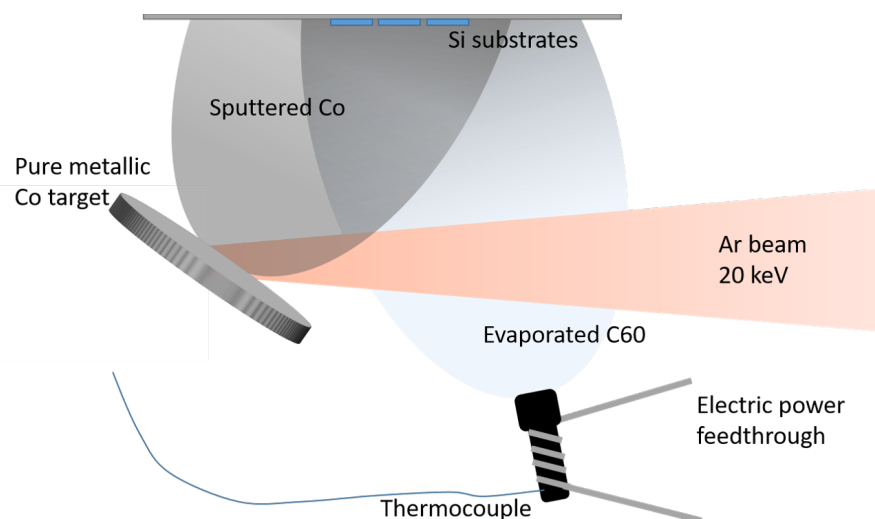


Figure 1. Deposition scheme with IBS setup and thermal evaporator

backscattering angle of 170° out of the plane, in accordance with Cornell geometry. In the ERDA measurement, He^+ ions with an energy of 2.5 MeV were utilized to identify H, and the detector was placed at a backscattering angle of 30° in the plane, following the IBM geometry. The recoiled particles were detected by a Canberra PIPS detector preceded by a $12\ \mu m$ thick Mylar foil. Data obtained by ion beam analysis were processed using the SIMNRA code [41]. The irradiation of the samples by means of a continuous beam of Ar^+ was carried out using the LEIF (NPI) system, positioning the samples orthogonal to the beam in place of the sputtering target. For irradiation, an energy of 20 keV and a current of $500\ \mu A$ were used up to a total fluence of $1E15\ Ar/cm^2$. Another sample set was irradiated at the same fluence and energy using a pulsed C^+ beam. A Laser Ion Source (Nagaoka University) was used to produce a pulsed C beam. The used laser source was a Quantel Brilliant operating at 10Hz repetition rate, 6ns pulse duration, 532 nm wavelength and laser energy of 130 mJ. The laser pulse was focused (in vacuum) on the surface of a C target held at a voltage of 20kV and facing the grounded samples. To reach the same fluence used for the Ar beam, a total of 12000 pulses were needed for each sample. An additional set of samples was exposed directly to the laser source, to induce changes on the surface. The laser irradiations occurred in air, without laser focusing and at an energy of 5 mJ per pulse. Each sample was irradiated with 1000 pulses. The annealing was performed using a special vacuum chamber with a heating system inside. The annealing was performed in a vacuum level of $1E-5$ mbar and for a duration of 5h (without considering the cooling time) at temperature of $300^\circ C$. The samples, pristine and modified, were investigated for morphological evolution by scanning electron microscopy SEM Hitachi-SU8230. Additional morphological study with elemental mapping of the materials was carried out using the Thermo Scientific Helios™ 5 UC Dual Beam Scanning Electron Microscope (SEM-FEG-UHR) equipped with different detector ETD (Everhart-Thornley Detector), TLD (Through-the-Lens) and STEM (Scanning Transmission Electron Microscopy). The elemental analysis and mapping were carried out by using the energy dispersive analysis system (EDX). Measurements were carried out with an operating voltage between 10 and 30 kV, without pretreatment of the samples. The TEM analysis of microstructure was performed by use of Jeol 2200 FS (Jeol, Tokio, Japan) field emission gun (FEG) equipped with with an Oxford Instruments EDS analyzer, instrument operating at a 200 kV accelerating voltage with a point resolution of $2.4\ \text{\AA}$. The micrographs have been carried out using a TVIPS camera and EM-Menu software.

Raman spectroscopy measurements were also performed, using a LabRam HR-EVO Horiba operating at 532 nm, 50X LWD with power $0.8\ mW$ per μm^2 and CCD Syncerity Horiba and NRS 7200 microRaman spectrometer with 532 nm wavelength and applied power $6.5\ mW$. In particular, the micro-Raman spectrometer was used for the evaluation of the as-deposited and modified films, on the other hand the Raman spectrometer was used for the fullerene characterization. Changes in electrical resistivity of the pristine and modified samples, were investigated using 2182A Nanovoltmeter and 6221 DC current source Keithley on the surface of sample, in a galvanostatic setup. The measurements were performed using the standard two-point method in air and room temperature. While the two-point method includes contact and lead resistances, all measurements were performed under identical conditions, allowing reliable comparison of relative resistance

changes induced by different treatments.

3 Results

The chemical composition of the produced films was investigated after deposition using Rutherford Backscattering Spectrometry (RBS) and Elastic Recoil Detection Analysis (ERDA) techniques. These scattering techniques are used for compositional thin film analysis, based on stopping power and inelastic energy loss during ion-solid interactions and the kinematically recoil. In our case, RBS is particularly suitable for the detection of heavy Co atoms (because light C atoms are hidden by Silicon signal), meanwhile the ERDA is used for H detection. Experimental results relative to 2 MeV He^+ are shown in Fig. 2 with simulated fit. Note that the spectra were normalized to the substrate. Carbon measurements were performed using 1.735 MeV H^+ ions and different incident ions angle (0 degrees were used for measurement with He^+ analysis and 7 degrees for the H^+). The relative spectra are illustrated in Fig. S1 of the Supplementary information (SI). Table 1 includes all the elemental concentrations' values of the data acquired by performing RBS and ERDA analyses on Co and Co - C_{60} films. RBS measurements confirm that CoC_{60} hybrid films have been successfully fabricated.

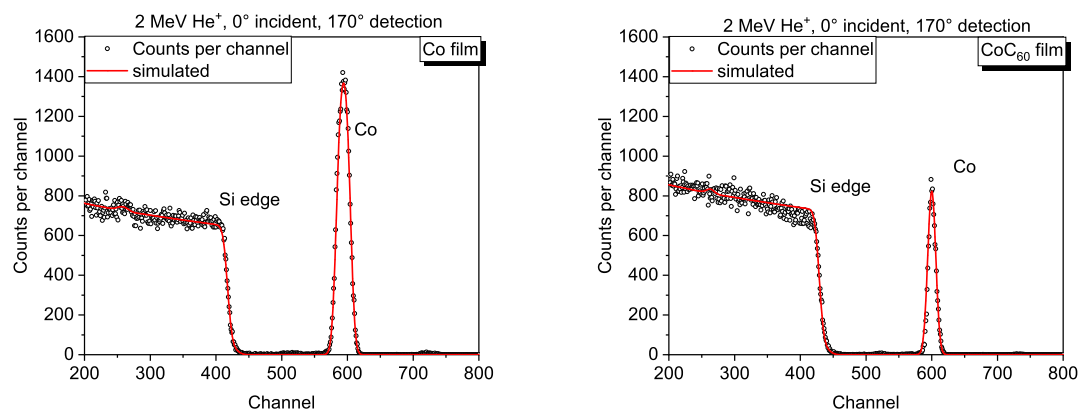


Figure 2. RBS results on pure Co and Co - C_{60} samples obtained with 2MeV He^+ . Black dots are experimental data and the red line represents the fit obtained from SIMNRA simulation.

Table 1. Elemental composition of samples calculated by RBS-ERDA analysis using both 2MeV He^+ beam and 1.735 MeV H^+ .

Sample	Co [at. %]	C [at. %]	O [at. %]	H [at. %]	Thickness [10^{15} at/cm 2]
Co film	70	14	5	11	480
Co - C_{60} film	50	33	3	14	245

Oxygen and carbon contaminations as well as hydrogen content are detected in the produced films. The sample with C_{60} show almost a ratio 3:2 between Co and C atoms. It should be noted that the pure Co film was prepared and analyzed exclusively as a compositional and structural reference for ion beam analysis. The electrical, morphological, and post-treatment comparisons discussed in this work are performed only among Co- C_{60} hybrid films, which share the same deposition conditions and comparable thickness. Therefore, the difference in areal density between pure Co and Co- C_{60} films does not introduce bias in the comparative interpretation of the hybrid film properties.

Presence of oxygen in the deposited films can be explained as oxidation of the Co NPs (possibly formed in the film nanostructure) during the air exposure of the samples.

The quantity of oxygen is independent of the presence of C_{60} or the ratio between Co and C_{60} . This may suggest that the detected oxygen is bounded chemically to the cobalt, forming more realistic composition $Co_xO_yC_{60}$. By coming into contact with the Co clusters, the O_2 molecules react with the Co surface causing O_2 dissociation and formation of the Co_xO_y [42]. By considering that the presence of C atoms in pure Co film (due to vacuum contamination by partial sputter of holder and shutter probably) and Co- C_{60} film are 14% and 33%, respectively, we can confirm that the C_{60} is almost the 20% of the film, so the majority of the film consists of Co atoms. As

illustrated in Fig. S2 of SI, the RBS analysis allows us to also establish that the distributions of Co and C, as well as the other elements, within the thickness of the samples are constant. Furthermore, thanks to the ERDA results, the presence of about 10% of H atoms was measured and confirmed as shown later by Raman analysis.



Figure 3. SEM pictures taken at 50kX magnification of as deposited sample.

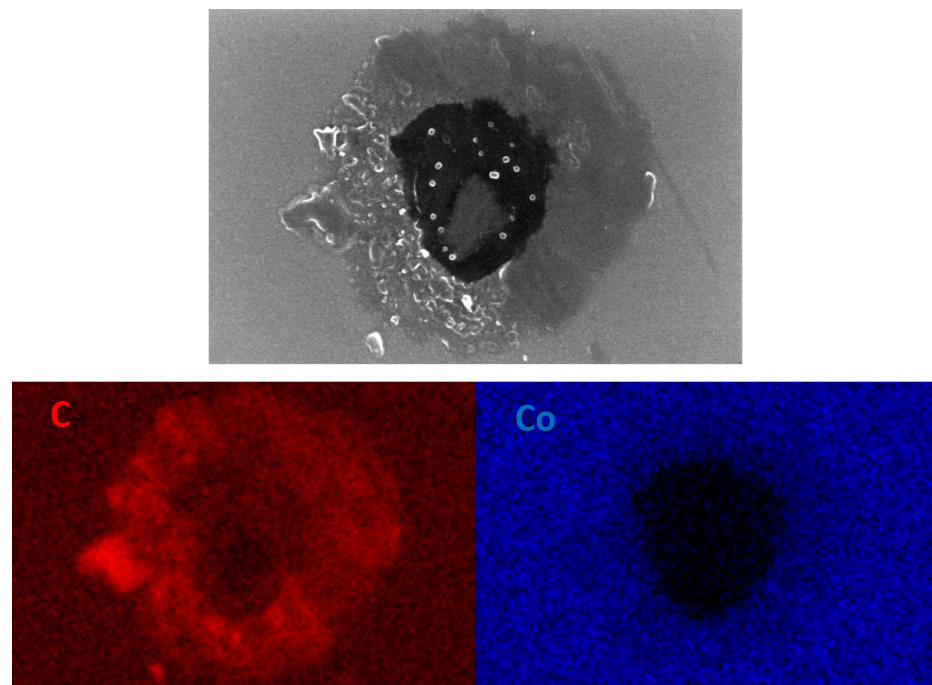


Figure 4. Elemental mapping of particle on the as deposited sample.

Fig.3 reports the SEM images for the as prepared samples and Fig.4 shows elemental mapping of selected particles obtained using EDX analysis. In the SEM micrograph of pristine sample, smooth surface and uniform particles distribution are recognized, indicating homogeneous mixture with few visible micron sized particles. EDX analyses reported in Fig.4 were performed on a selected particle to understand its composition. It was found a deficiency of Co inside the particle with a Co-enriched ring around it, and uniform distribution anywhere else. In order to observe the formed nanostructures in the hybrid CoC₆₀ films, we performed detailed TEM analyses on the as deposited film. So, following the procedure reported in the “Materials and Methods” section, we deposited the sample on Cu holey carbon grid to analyze it for structural information. Fig.5 shows the TEM image obtained from the CoOC₆₀ film. The sample has composite nanostructure consisting of small Co nanoparticles distributed uniformly. Samples subject to modification were analyzed from morphological point of view as the pristine one. The SEM images from the modified samples are reported in Fig.6 taken at a magnification of 2.5kx. For each of these samples was performed as well elemental mapping with EDX analysis on selected particles.

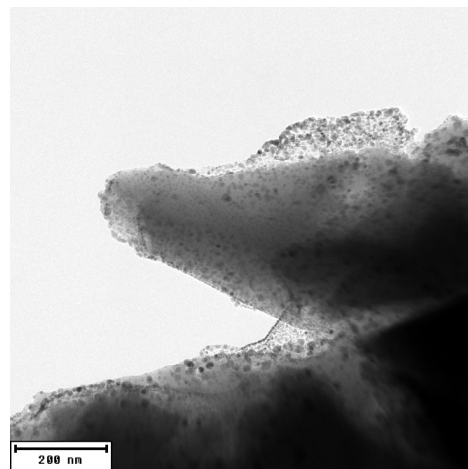


Figure 5. TEM micrograph of as prepared sample.

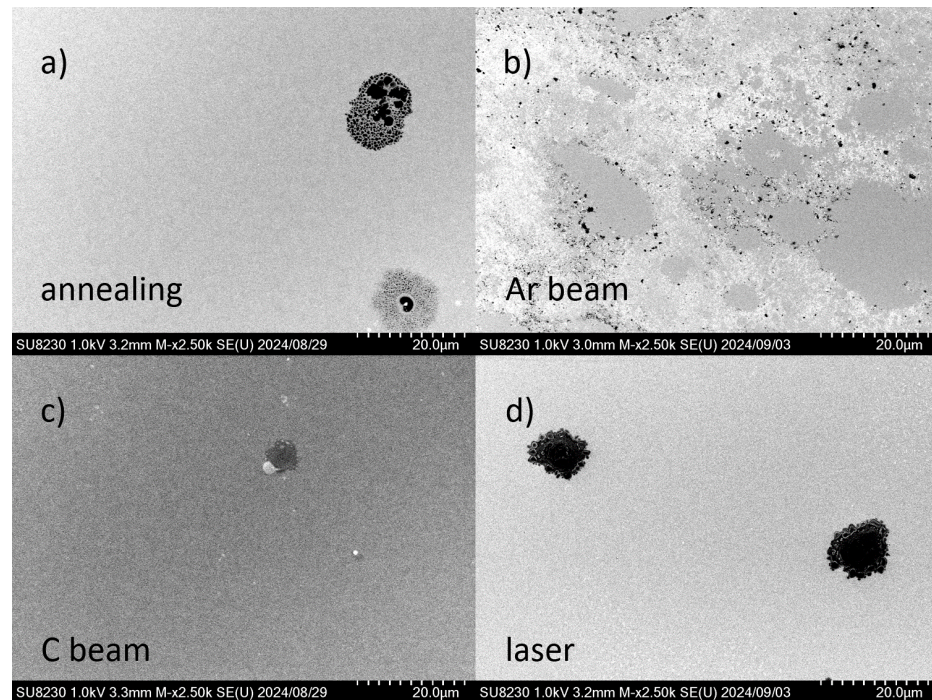


Figure 6. SEM pictures taken at 2.5kX magnification modified samples.

All treatments applied to the films to alter their properties and morphologies resulted in the development of numerous structures on the surface. One of the possible reasons behind these phenomena is the stress accumulated on the surface (and immediately under the surface) during the deposition, due to the immiscibility of the materials. This stress is released almost instantaneously with the treatments, creating separation of the phases. The energy in excess, provided by the treatment is used for the growth of structures around the nucleation point. Depending on the available energy, more or less organized structures can form.

From the large area SEM, the sample that was subjected to annealing (Fig. 6a) presents structures tending to the circular shape, with a strong nucleation of C_60 above the Co (or viceversa). Some structures show a main nucleation surrounded by a huge number of smaller nucleations (see Fig. S3 of SI for additional pictures). The sample exposed to Ar^+ beam irradiation (Fig. 6b) displays a great number of very small separation spots, non-organized and spread randomly on the surface (see Fig. S4 of SI for additional pictures). The C^+ irradiation (Fig. 6c) did not produce a particular separation on this films surface at least visible, but possible compositional changes in the C phase (see Fig. S5 of SI for additional pictures). The laser irradiation showed in Fig. 6d produced large spots with C nucleation, but also microstructures

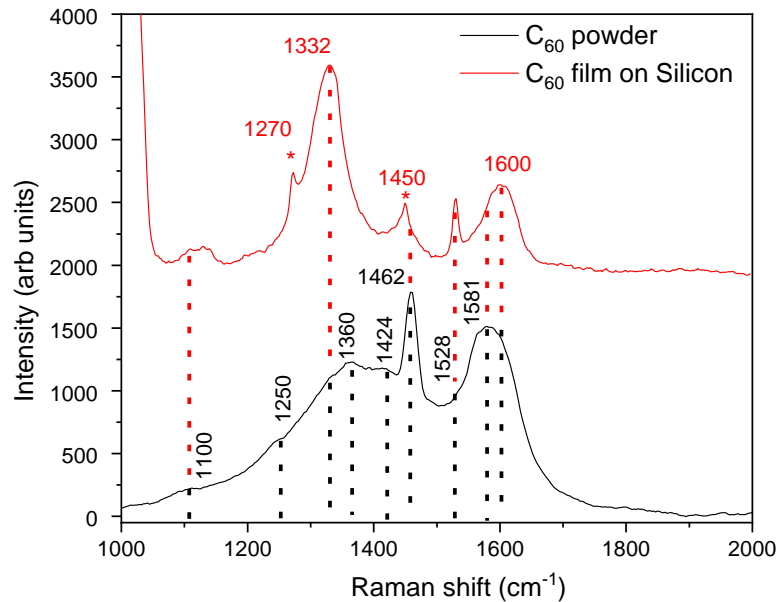


Figure 7. Raman spectrum of C_{60} powder (black line) and C_{60} film deposited onto silicon substrate (red line). Peaks exclusive to the C_{60} film spectrum are marked with asterisks, while the dotted lines (black and red) highlight peaks common to both C_{60} powder and film.

with resemblance of long crystal structures (see Fig. S6 of SI for additional pictures). The EDX mapping shows that the agglomerations of particles are formed by both constituents, with little more content of C in the center. Compared with the pristine sample there is the elemental distributions are more homogeneous, due to the release of existing stress. Additional EDX mapping are shown in SI Fig. S7-10.

A detailed Raman analysis of the pristine films of pure and hybrid materials was performed. Fig. 7 shows the Raman spectra of the C_{60} film deposited on the silicon substrate, compared to the vibrational fingerprint of pure C_{60} powder used as a precursor in film preparation, obtained by excitation with a 532 nm laser wavelength. The Raman spectrum of the C_{60} powder (black line) displays several Raman contributions between 1000 and 2000 cm^{-1} , closely matching values found in the literature [43, 44]. Notably the Raman-active modes of H_g symmetry are found at ~ 1100 cm^{-1} ($H_g(5)$), ~ 1250 cm^{-1} ($H_g(6)$), ~ 1424 cm^{-1} ($H_g(7)$), and 1581 cm^{-1} ($H_g(8)$). In this Raman shift region, the peak at 1462 cm^{-1} is assigned to the $A_g(2)$ mode, known as “pentagonal pinch” since caused by the contraction of the pentagonal rings and the expansion of the hexagonal rings of carbon atoms. These peaks overlay the broader bands observed in the spectral ranges of 1330 – 1360 cm^{-1} and 1560 – 1600 cm^{-1} , corresponding to the D and G bands, respectively, which are characteristic of all carbon-based materials under visible-range excitation [45]. Notably, laser heating during Raman measurements can facilitate the formation of additional carbon phases.

The complete spectrum of C_{60} powder, which includes the remaining four low-frequency H_g symmetry modes and the purely radial $A_g(1)$ mode at 496 cm^{-1} , is shown in Fig. S11 of the Supplementary Information. The Raman spectrum of C_{60} film (red line in Fig. 7) shows a distinctive peak at 1450 cm^{-1} (highlighted by asterisk), which attests a photo-transformed state of C_{60} and the presence of polymer chains that, in the case of film, easily form during laser irradiation in Raman measurements [43]. Furthermore, the $A_g(2)$ peak at 1462 cm^{-1} , characteristic of the C_{60} powder, almost disappears in the fullerene film as it is overshadowed by the tail of the prominent peak at 1450 cm^{-1} . It is worthy to note the presence of the wide D band mainly peaked at 1332 cm^{-1} , typical of diamond-like carbon materials. The peak at 1270 cm^{-1} (highlighted by asterisk) is ascribed to a combination of antisymmetric C-C interring stretching mode and antisymmetric bending mode of C-H groups that form on fullerene surface [46]. The prominent and sharp peak tail that diminishes at 1065 cm^{-1} corresponds to the second-order Raman peak of the Si substrate. Fig. 8 displays the Raman spectra of hybrid Co- C_{60} films, both pristine and post-treatment, within the 800 – 1800 cm^{-1} spectral range. Notably, the characteristic $A_g(2)$ peak at 1462 cm^{-1} is significantly broadened and overlaps with the D and G bands (at 1360 and 1562 cm^{-1} , respectively), which are

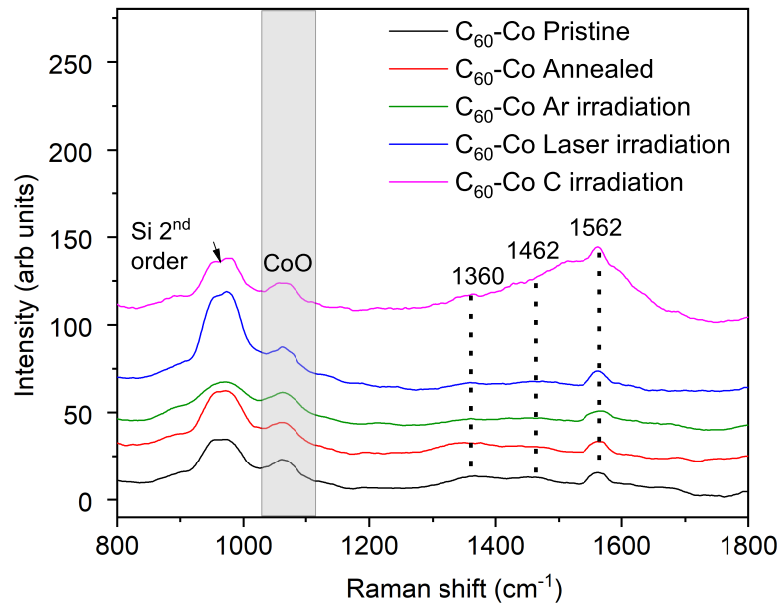


Figure 8. Raman spectra of hybrid Co-C₆₀ films, as deposited (black line) onto silicon substrate and post-treatments: Co-C₆₀ film annealed (red line), Co-C₆₀ film Ar irradiated (green line), Co-C₆₀ film laser irradiated (blue line), and Co-C₆₀ film C irradiated (magenta line). The spectra are stacked in intensity for a better visualization.

typical features of carbon materials. When the Co-C₆₀ is irradiated by carbon beam, a pronounced broad band appears beneath this peak, which is attributed to the formation of amorphous carbon. Furthermore, all spectra exhibit a broad band in the spectral range between 1030 and 1100 cm^{-1} (grey rectangle in Fig. 8), attributed to the second-order two-phonon Raman scattering of the CoO phase [47]. This spectral feature indicates cobalt oxidation induced in defective sites of cobalt during the co-deposition of hybrid films. Under laser heating during Raman measurements, the CoO phase readily transforms into the Co₃O₄ phase [48].

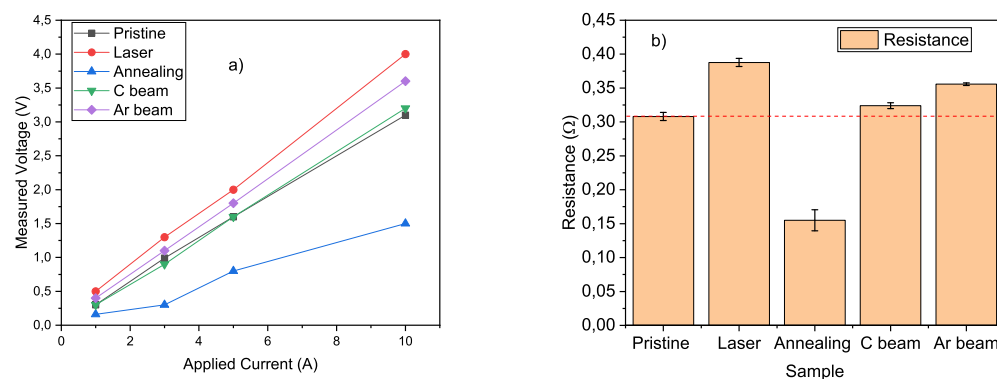


Figure 9. Results of galvanostatic measurement a) and calculated electrical resistance b), measured using 2-points method.

The results concerning the electrical resistance measurements performed on the films are shown in Fig. 9. Fig. 9a shows the galvanostatic measurements performed on the samples surface, using the setup described in "Material and Methods" section. The voltage measured with a nanovoltmeter between the electrodes that applied stabilized current to the films were recorded for several applied current values that ranged from 1 A to 10 A. Fig. 9b illustrates the resistance calculated by linear regression of the data in Fig. 9a. If we consider the pristine Co - C₆₀ film, it

shows a resistance of 0.308Ω . It is a valid assumption considering this value as the reference for all the deposited films when the samples were all produced together during the same deposition. In this way, the measured variations in the resistance values are due only to the treatments to which they were exposed. Irradiation with a laser beam as well as bombardment with charged particles increased the resistance of the samples. In particular, laser irradiation leads to the highest resistance observed. An interesting result is instead the one referring to the sample subjected to annealing, for which the resistance value is 0.155Ω , almost half of the thin film in the pristine state. Probably, the annealing process produces large enucleations of C_{60} , separating the metal from the fullerene more clearly and the reduction in resistance observed after annealing is attributed to phase segregation and morphological reorganization, which likely promotes the formation of percolative Co-rich conduction pathways, even in the presence of partial cobalt oxidation.

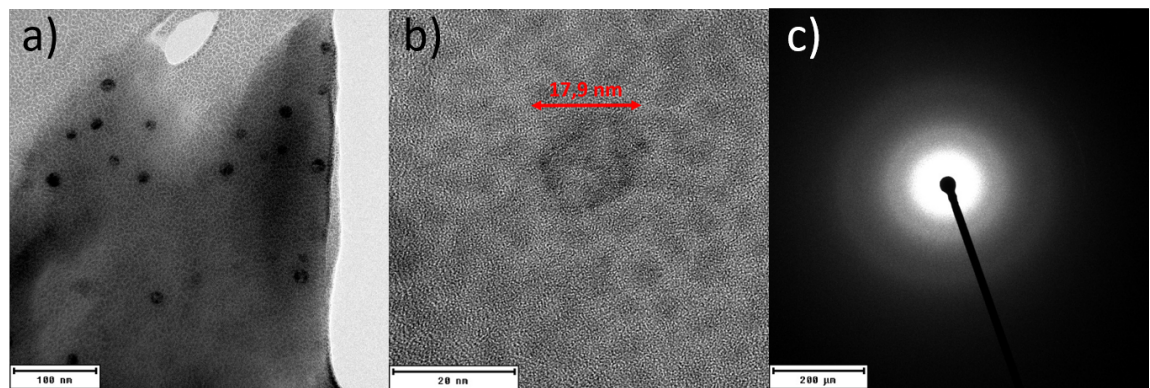


Figure 10. TEM micrograph of annealed sample, magnification of fullerene NPs and SAED of area in picture.

In order to investigate the origin of these particular electrical properties of the annealed samples, additional structural analyses were performed with TEM and the Selected Area Electron Diffraction (SAED) method on the grid sample. Fig.10a) shows the morphology of selected area of modified film. It is possible to see agglomerations of self-assembled C_{60} nanoparticles of the size of 17.9 nm (Fig.10b). Instead, the SAED analysis allows us to measure the lattice parameters, crystal structure, and extent of crystallinity of nanoparticles from the diffraction technique, in which the sample is targeted with a parallel beam of high energy electrons. In particular, Fig.10c) illustrates that the film is in an amorphous state as expected. Finally, this area of the annealed grid sample was selected to perform elemental mapping also with the aim of understanding the elemental distribution of the elements (Fig.11). As shown by the oxygen mapping, Cobalt effectively becomes oxidized, so the reduced electrical resistance has to be ascribable to a self-agglomeration of C_{60} fullerene. Unfortunately, the carbon distribution is affected by the holey C film on which it is deposited.

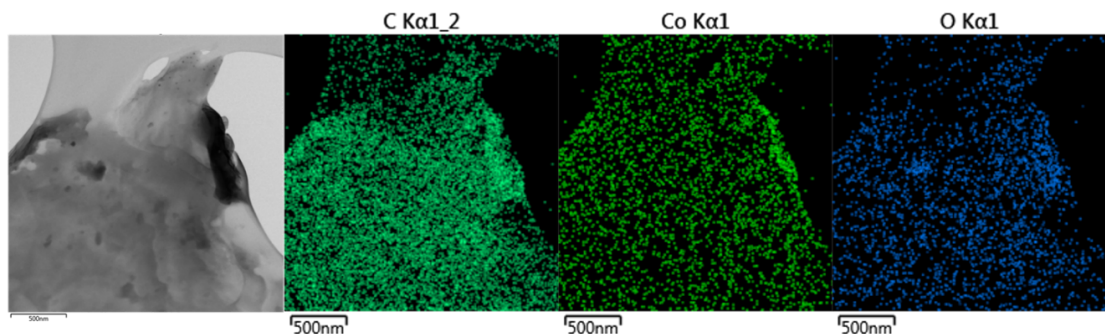


Figure 11. Elemental mapping of area shown in Fig.10

Discussion

The systematic study performed in this work is focused on the preparation of Co–C₆₀ hybrid films under identical growth conditions and on their controlled modification through multiple external stimuli, enabling a direct comparison of distinct post-treatment pathways and their effects on nanostructure and functional properties. Well established ion beam analytical techniques, such as RBS and ERDA, have been used in the study to evaluate the film's original composition and thickness. “As deposited” and modified samples revealed several important morphological and structure evolutions based on the applied external stimuli.

During the self-assembly of fullerene nanoparticles in a nonequilibrium solid-solution, C₆₀ molecules form a nanoparticle, finding the most advantageous combination of interactions between molecules with minimal free energy. Considering the efforts usually required to prepare the nanoparticle by pulverization, the possibility to obtain nanosized C₆₀ by dry physical method (in our case thermal evaporation) is truly an innovative result, considering that self-aggregation process of C₆₀ particles is purely physical, and is not associated with visible changing in phase crystal structure. Interesting physical and structural properties were observed in the metal-C₆₀ phase without and with separation induced by external perturbations. SEM analyses performed on treated samples showed strong separations of the immiscible phases. The magnitude of such separations was different for each applied perturbation, as well as for the final shapes of formed structures. The nucleation produced by some treatments (e.g., the annealing process) produced a quasi-perfect circular germination of the material surrounded by smaller separation areas. These strong separations sometimes occur with neither the growth of carbon structures above the film nor with the formation of cobalt structures above the film. The study conducted using Raman spectroscopy allowed for the identification of the characteristic C₆₀ peak in the deposited film without Co, confirming the presence of the hollow structure of the fullerene. When combined with Co, there was a broadening of the characteristic A_g(2) peak, with an overlapping of D and G bands. In particular, it was observed that after carbon irradiation, a pronounced broad band appears beneath this peak due to the strong amorphization of carbon. The band attributed to the oxides of cobalt are also detected revealing a transformation of CoO in Co₃O₄ phase, as confirmed by Rivas-Murias and Salgueiríño in their previous work [48]. Despite the presence of cobalt oxides, electrical resistance measurements revealed a non-monotonic response to the applied treatments. Ion and laser irradiation resulted in an increase in resistance, consistent with enhanced disorder, amorphization, and oxidation effects. In contrast, thermal annealing led to a pronounced reduction in the measured resistance in comparison to the pristine film. This behavior cannot be attributed to simple increase of Co amount, as oxidation of cobalt is clearly evidenced by Raman spectroscopy and elemental mapping. Instead, the reduced resistance observed after annealing is to be attributed to morphology-driven reorganization and phase segregation within the hybrid film. TEM analysis of the annealed samples reveals the formation of self-assembled C₆₀ nanoparticles, indicating substantial molecular rearrangement and separation of the fullerene- and cobalt-rich regions. In such heterogeneous systems, cobalt is likely present in a mixed state comprising oxidized surface or interfacial regions surrounding Co-rich cores. In this case, electrical transport is governed by formation conduction pathways, where the macroscopic resistance is dominated by the connectivity of the most conductive regions rather than by the average phase composition.

Therefore, even in the presence of partial cobalt oxidation and intrinsically low fullerene conductivity, phase segregation induced by annealing can promote the formation of effective Co-rich conduction paths, resulting in a lower measured resistance. Overall, this study provides a comparative framework for understanding how different energy-delivery mechanisms affect Co–C₆₀ hybrid systems. The post-treatment-focused approach presented here offers a valuable strategy for tailoring the functional properties of metal–organic hybrid films and can be extended to other immiscible composite systems relevant to electronics, spintronics, and energy-related applications.

Acknowledgments

Sample text inserted for demonstration.

Funding

The authors acknowledge the financial support from the MEYS CR, Project OP JAK FerrMion, No. CZ.02.01.01/00/22_008/0004591. The authors acknowledged also the support of Czech Academy of Science Mobility Plus Project, Grant No. JSPS-24-12 and JSPS Bilateral Program Number JPJSBP120242501. Measurements were carried out at the CANAM infrastructure of the NPI CAS Rez under project LM 2015056. B.F. acknowledges the Italian Project PNRR “I-PHOQS - Integrated Infrastructure Initiative in Photonic and Quantum Sciences, CUP B53C22001750006.”

Part of this research was conducted within the activities of the RTD-A contract of S. Vasi co-funded by PON ‘Ricerca e Innovazione’ 2014-2020 (PON R&I FSE-REACT EU), Azione IV.6 ‘Contratti di ricerca su tematiche Green’. C.C. acknowledges the financial support by the European Union – NextGeneration EU PNRR IR0000020 ECCSELLENT through NRRP – M4C2, Inv. 3.1 “Development of ECCSEL-R.I. Italian facilities: user access, services and long-term sustainability”

Author contributions

G.C and K.T. conceived the experiment, G.C. and J.V. performed the samples preparation, G.C., E.S., K.T., Y.K., and R.M. conducted the experiment of sample modification, B.F., S.V., C.C., A.M., R.M. and P.M. and J.N. performed the analysis, R.M., Y.K., S.V. analyzed the results, S.V., B.F. and G.C. manuscript preparation. All authors reviewed the manuscript.

Data availability

Sample text inserted for demonstration.

Supplementary data

Sample text inserted for demonstration.

References

- [1] M. Scheele, W. Brütting, and F. Schreiber. Coupled organic–inorganic nanostructures (COIN). *Physical Chemistry Chemical Physics*, 17(1):97–111, 2015.
- [2] Elizabeth Goiri, Patrizia Borghetti, Afaf El-Sayed, J. Enrique Ortega, and Dimas G. de Oteyza. Multi-Component Organic Layers on Metal Substrates. *Advanced Materials*, 28(7):1340–1368, December 2015.
- [3] Yuanjing Cui, Bin Li, Huajun He, Wei Zhou, Banglin Chen, and Guodong Qian. Metal–Organic Frameworks as Platforms for Functional Materials. *Accounts of Chemical Research*, 49(3):483–493, February 2016.
- [4] Jagannath Devkota, Rugang Geng, Ram Chandra Subedi, and Tho Duc Nguyen. Organic spin valves: A review. *Advanced Functional Materials*, 26(22):3881–3898, March 2016.
- [5] R. Otero, A.L. Vázquez de Parga, and J.M. Gallego. Electronic, structural and chemical effects of charge-transfer at organic/inorganic interfaces. *Surface Science Reports*, 72(3):105–145, July 2017.
- [6] Joshua D. Sosa, Timothy F. Bennett, Katherine J. Nelms, Brandon M. Liu, Roberto C. Tovar, and Yangyang Liu. Metal–Organic Framework Hybrid Materials and Their Applications. *Crystals*, 8(8):325, August 2018.
- [7] Xiaoyu Song, Xinyue Wang, Yusen Li, Chengzhi Zheng, Bowen Zhang, Chong-an Di, Feng Li, Chao Jin, Wenbo Mi, Long Chen, and Wenping Hu. 2D Semiconducting Metal–Organic Framework Thin Films for Organic Spin Valves. *Angewandte Chemie International Edition*, 59(3):1118–1123, November 2019.
- [8] Marcela Socol, Nicoleta Preda, Andreea Costas, Bogdana Borca, Gianina Popescu-Pelin, Andreea Mihailescu, Gabriel Socol, and Anca Stanculescu. Thin Films Based on Cobalt Phthalocyanine:C60 Fullerene:ZnO Hybrid Nanocomposite Obtained by Laser Evaporation. *Nanomaterials*, 10(3):468, March 2020.
- [9] Zhichao Shao, Junshuai Chen, Kexin Gao, Qiong Xie, Xiaojing Xue, Xue Li, Hongwei Hou, and Liwei Mi. A high-spintronic helix metal–organic chain as a high-output triboelectric nanogenerator material for self-powered anticorrosion. *Chemical Engineering Journal*, 455:140865, January 2023.
- [10] Rostislav Langer, Kimmo Mustonen, Alexander Markevich, Michal Otyepka, Toma Susi, and Piotr Błoński. Graphene lattices with embedded transition-metal atoms and tunable magnetic anisotropy energy: implications for spintronic devices. *ACS Applied Nano Materials*, 5(1):1562–1573, 2022.
- [11] Pin-Cheng Lin, Renan Villarreal, Simona Achilli, Harsh Bana, Maya N Nair, Antonio Tejeda, Ken Verguts, Stefan De Gendt, Manuel Auge, Hans Hofäss, et al. Doping graphene with substitutional mn. *ACS nano*, 15(3):5449–5458, 2021.

- [12] Jiong Wang, Liyong Gan, Wenyu Zhang, Yuecheng Peng, Hong Yu, Qingyu Yan, Xinghua Xia, and Xin Wang. In situ formation of molecular Ni-Fe active sites on heteroatom-doped graphene as a heterogeneous electrocatalyst toward oxygen evolution. *Science advances*, 4(3):eaap7970, 2018.
- [13] Dehui Deng, KS Novoselov, Qiang Fu, Nanfeng Zheng, Zhongqun Tian, and Xinhe Bao. Catalysis with two-dimensional materials and their heterostructures. *Nature nanotechnology*, 11(3):218–230, 2016.
- [14] Qiaoqiao Zhang and Jingqi Guan. Single-atom catalysts for electrocatalytic applications. *Advanced Functional Materials*, 30(31):2000768, 2020.
- [15] Diego Cortés-Arriagada, Nery Villegas-Escobar, and Daniela E Ortega. Fe-doped graphene nanosheet as an adsorption platform of harmful gas molecules (CO, CO₂, SO₂ and H₂S), and the co-adsorption in O₂ environments. *Applied Surface Science*, 427:227–236, 2018.
- [16] Miao Zhou, Yun-Hao Lu, Yong-Qing Cai, Chun Zhang, and Yuan-Ping Feng. Adsorption of gas molecules on transition metal embedded graphene: a search for high-performance graphene-based catalysts and gas sensors. *Nanotechnology*, 22(38):385502, 2011.
- [17] H Tanaka, K Marumoto, S Kuroda, T Ishii, R Kanehama, N Aizawa, H Matsuzaka, K Sugiura, H Miyasaka, T Kodama, K Kikuchi, I Ikemoto, and M Yamashita. Electron spin resonance studies of Co(tbp) · C₆₀single crystal. *Journal of Physics: Condensed Matter*, 14(15):3993–4000, April 2002.
- [18] Dmitri V. Konarev, Salavat S. Khasanov, Gunzi Saito, Rimma N. Lyubovskaya, Yukihiro Yoshida, and Akihiro Otsuka. The Interaction of C₆₀, C₇₀, and C₆₀(CN)₂ Radical Anions with Cobalt(II) Tetraphenylporphyrin in Solid Multicomponent Complexes. *Chemistry - A European Journal*, 9(16):3837–3848, August 2003.
- [19] Genki Yoshikawa, Yuki Tsuruma, Susumu Ikeda, and Koichiro Saiki. Noble Metal Intercalated Fullerene Fabricated by Low-Temperature Co-deposition. *Advanced Materials*, 22(1):43–46, December 2009.
- [20] Ritu Vishnoi, Satakshi Gupta, Umesh Kumar Dwivedi, and Rahul Singhal. Optical and structural modifications of copper-fullerene nanocomposite thin films by 120 MeV Au ion irradiation. *Radiation Physics and Chemistry*, 166:108442, 2020.
- [21] Agnieszka Karczmarska, Michał Adamek, Sara El Houbbadi, Paweł Kowalczyk, and Magdalena Laskowska. Carbon-supported noble-metal nanoparticles for catalytic applications—a review. *Crystals*, 12(5):584, 2022.
- [22] Gaurang Joshi, Kush P Mehta, et al. Fabrication and applications of fullerene-based metal nanocomposites: A review. *Journal of Materials Research*, 36(1):114–128, 2021.
- [23] Dinesh Varshney, Meenu Varshney, RK Singh, and Raghvendra Mishra. Superconductivity in alkali metal doped fullerenes (K₃C₆₀): a phonon mechanism. *Journal of Physics and Chemistry of Solids*, 60(5):579–585, 1999.
- [24] Hiroyuki Takeya, Ryoei Kato, Takatsugu Wakahara, Kun'ichi Miyazawa, Takahide Yamaguchi, Toshinori Ozaki, Hiroyuki Okazaki, and Yoshihiko Takano. Preparation and superconductivity of potassium-doped fullerene nanowhiskers. *Materials Research Bulletin*, 48(2):343–345, 2013.
- [25] J. Vacik, V. Lavrentiev, K. Novotna, L. Bacakova, V. Lisa, V. Vorlicek, and R. Fajgar. Fullerene (C₆₀)-transitional metal (Ti) composites: Structural and biological properties of the thin films. *Diamond and Related Materials*, 19(2–3):242–246, February 2010.
- [26] A.S. Bolokang, M.J. Phasha, S.T. Camagu, D.E. Motaung, and S. Bhero. Effect of thermal treatment on mechanically milled cobalt powder. *International Journal of Refractory Metals and Hard Materials*, 31:258–262, March 2012.
- [27] Sonia Kaushik, Avinash G. Khanderao, Pooja Gupta, V. Raghavendra Reddy, and Dileep Kumar. Growth of ultra-thin Cobalt on fullerene (C₆₀) thin-film: in-situ investigation under UHV conditions. *Materials Science and Engineering: B*, 284:115911, October 2022.

[28] Suraj Gupta, Rohan Fernandes, Rupali Patel, Matjaž Spreitzer, and Nainesh Patel. A review of cobalt-based catalysts for sustainable energy and environmental applications. *Applied Catalysis A: General*, 661:119254, July 2023.

[29] Gauravkumar Patel, Fabian Ganß, Ruslan Salikhov, Sven Stienen, Lorenzo Fallarino, Rico Ehrler, Rodolfo A. Gallardo, Olav Hellwig, Kilian Lenz, and Jürgen Lindner. Structural and magnetic properties of thin cobalt films with mixed hcp and fcc phases. *Physical Review B*, 108(18):184429, November 2023.

[30] GH Lee, SH Huh, JW Jeong, and H-C Ri. Excellent magnetic properties of fullerene encapsulated ferromagnetic nanoclusters. *Journal of magnetism and magnetic materials*, 246(3):404–411, 2002.

[31] Andrew Kuznetsov. Magnetic properties of endohedral complexes $\text{Co}_5 @ \text{C}_n$ depending upon the size and symmetry of fullerenes as well as orientation of cobalt cluster. *Computational Materials Science*, 54:204–207, 2012.

[32] Giovanni Ceccio, Jiri Vacík, Vasyl Lavrentiev, Ivo Tomandl, Romana Miksova, and Kazumasa Takahashi. Study of thin film composites based on LiCoO_2 and C_{60} using neutron depth profiling and atomic force microscopy. *Journal of Radioanalytical and Nuclear Chemistry*, 333(12):6687–6697, 2024.

[33] J Vacík, V Lavrentiev, V Havranek, P Horák, V Hnatowicz, and R Fajgar. Laser-induced periodic surface structure in nickel–fullerene composites. *Radiation Effects and Defects in Solids*, 171(1-2):154–160, 2016.

[34] Michal Zalibera, Frank Ziegs, Sandra Schiemenz, Vasilii Dubrovin, Wolfgang Lubitz, Anton Savitsky, Shihu HM Deng, Xue-Bin Wang, Stanislav M Avdoshenko, and Alexey A Popov. Metallofullerene photoswitches driven by photoinduced fullerene-to-metal electron transfer. *Chemical Science*, 12(22):7818–7838, 2021.

[35] J Vacík, V Lavrentiev, V Hnatowicz, V Vorlický, and H Naramoto. Hybridization And Modification Of The Ni/ C_{60} Composites. In *AIP Conference Proceedings*, volume 1099, pages 553–556. American Institute of Physics, 2009.

[36] Seiji Sakai, Hiroshi Naramoto, Pavel V Avramov, Tsuyoshi Yaita, Vasily Lavrentiev, Kazumasa Narumi, Yuji Baba, and Yoshihito Maeda. Comparative study of structures and electrical properties in cobalt–fullerene mixtures by systematic change of cobalt content. *Thin Solid Films*, 515(20-21):7758–7764, 2007.

[37] V Lavrentiev, M Motylenko, M Barchuk, C Schimpf, I Lavrentieva, J Pokorný, C Röder, J Vacík, A Dejneka, and D Rafaja. Structure assembly regularities in vapour-deposited gold–fullerene mixture films. *Nanoscale Advances*, 2(4):1542–1550, 2020.

[38] Vasily Lavrentiev, Dagmar Chvostova, Jan Pokorný, Inna Lavrentieva, Jiri Vacík, and Alexandr Dejneka. Tuneable interplay of plasmonic and molecular excitations in self-assembled silver–fullerene nanocomposites. *Carbon*, 184:34–42, 2021.

[39] Vasily Lavrentiev, Dagmar Chvostova, Mariana Klementova, Karla Kulsova, Esther de Prado, Jiri Vacík, Inna Lavrentieva, and Alexandr Dejneka. Room temperature excitonic coupling in self-assembled copper–Fullerene hybrid films exposed to ambient air. *Carbon*, 226:119230, 2024.

[40] J Vacík, G Ceccio, V Lavrentiev, R Miksova, V Havranek, P Pleskunov, and A Cannavò. Study of surface morphology of Ag thin films prepared by sputtering and irradiation with keV Ar ion beam. *Radiation Effects and Defects in Solids*, 179(1-2):136–145, 2024.

[41] Matej Mayer. SIMNRA, a simulation program for the analysis of NRA, RBS and ERDA. In *AIP conference proceedings*, volume 475, pages 541–544. American Institute of Physics, 1999.

[42] B Klingenberg, F Grellner, D Borgmann, and G Wedler. Oxygen adsorption and oxide formation on Co (1120). *Surface science*, 296(3):374–382, 1993.

[43] MS Dresselhaus, G Dresselhaus, and PC Eklund. Raman scattering in fullerenes. *Journal of Raman Spectroscopy*, 27(3-4):351–371, 1996.

- [44] Annett Dorner-Reisel, Uwe Ritter, Jens Moje, Emma Freiberger, and Peter Scharff. Effect of fullerene C₆₀ thermal and tribomechanical loading on Raman signals. *Diamond and Related Materials*, 126:109036, 2022.
- [45] Andrea Carlo Ferrari and John Robertson. Resonant Raman spectroscopy of disordered, amorphous, and diamondlike carbon. *Physical review B*, 64(7):075414, 2001.
- [46] Eric JJ Martin, Nicolas Bérubé, Françoise Provencher, Michel Côté, Carlos Silva, Stephen K Doorn, and John K Grey. Resonance Raman spectroscopy and imaging of push–pull conjugated polymer–fullerene blends. *Journal of Materials Chemistry C*, 3(23):6058–6066, 2015.
- [47] Yang Li, Wenlan Qiu, Fan Qin, Hui Fang, Viktor G Hadjiev, Dmitri Litvinov, and Jiming Bao. Identification of cobalt oxides with Raman scattering and Fourier transform infrared spectroscopy. *The Journal of Physical Chemistry C*, 120(8):4511–4516, 2016.
- [48] Beatriz Rivas-Murias and Verónica Salgueiríño. Thermodynamic CoO - Co₃O₄ crossover using Raman spectroscopy in magnetic octahedron-shaped nanocrystals. *Journal of Raman Spectroscopy*, 48(6):837–841, 2017.